Cellulose (2014) 21:71–86
DOI 10.1007/s10570-013-0150-x

ORIGINAL PAPER

# Quantum chemical calculations of pristine and modified crystalline cellulose surfaces: benchmarking interactions and adsorption of water and electrolyte

**Philippe Bourassa · Jean Bouchard · Sylvain Robert**

Received: 28 August 2013 / Accepted: 12 December 2013 / Published online: 22 December 2013


**Abstract** In this study, we investigate the hydration of three different functional groups present on cellulose nanocrystal (CNC) surfaces: hydroxyls, carboxylates and sulphates by means of quantum chemical calculation. The performance of several density functional theory (DFT) functionals in reproducing, against higher level MP2 benchmark calculations, relevant non-covalent CNC interactions is also assessed. The effect of a sodium ion on the hydration of the surface functional groups was also investigated. Major restructuring of the hydrogen-bonding network within cellulose was found in the presence of a sodium ion. The calculated binding energy of water with a surface group ion pair was also greater, which indicates a greater hydrophilicity of CNC surfaces in the presence of adsorbed sodium. Cellulose hydrophilic surfaces (1 1 0) and (1 −1 0) were also calculated using DFT methods. The results indicate that the surfaces possess different electrostatic potential maps. Hydrogen bond restructuring is found on the chemically modified surfaces. The adsorption energy of water and electrolyte is also found to be different on each surface.

**Keywords** Cellulose nanocrystals · DFT · Solvation · Surface modification · Self-assembly · Non-covalent interactions

P. Bourassa · S. Robert (✉)
Centre de Recherche sur les Matériaux Lignocellulosiques, Université du Québec à Trois-Rivières, 3351 boulevard des Forges, Trois-Rivières, QC G9A 5H7, Canada
e-mail: sylvain.robert@uqtr.ca; robert@uqtr.ca

J. Bouchard
FPInnovations, 570 boulevard Saint-Jean, Pointe-Claire, QC H9R 3J9, Canada
e-mail: jean.bouchard@fpinnovations.ca

## Introduction

Cellulose is the most abundant biomaterial on earth. It is the main structural constituent of plants and is also found in various bacteria, fungi, algae and even animals (O'Sullivan 1997). In its crystalline form, cellulose can be found in two different configurations: Iα (Nishiyama et al. 2003) which is mostly present in algae and bacteria and the Iβ allomorph (Nishiyama et al. 2002) which can be obtained from woody biomass. Cellulose Iβ can be isolated from the natural wood fibres by acid hydrolysis, which leads to crystals of nanometric dimensions (Elazzouzi-Hafraoui et al. 2007). These crystals possess a large aspect ratio and their surfaces can be readily modified selectively on the C6 carbons for use in diverse applications, notably in the field of composite materials (Habibi et al. 2010; Moon et al. 2011). Both negatively charged sulphate (Beck-Candanedo et al. 2005) and carboxylate groups (Hirota et al. 2009) can be introduced to the surface of the nanocrystals. These modified CNC particles are found to be easily dispersible in water at neutral pH

(Beck et al. 2012; Montanari et al. 2005) and the resulting suspensions can be used to make solid films which display interesting optical properties (Revol et al. 1998). These films show iridescence specular reflection. The wavelength can be controlled by adding electrolytes to the suspension (Dong et al. 1996; Dong and Gray 1997; Beck et al. 2010).

The optical properties of cellulose nanocrystal films arises from its self-assembled chiral nematic liquid crystal structure (Pan et al. 2010; Eichhorn 2011; Klemm et al. 2011). This mesoscopic structure is retained upon drying the suspension to form the film (Liu et al. 2011). Other than the optical properties, the chiral nematic structure of CNC has been used as a template to induce chirality in mesoporous silica (Stein 2010; Shopsowitz et al. 2010) and carbon films (Asefa 2012). Such novel materials based on CNC's particular structure show potential applications in gas storage, asymmetric catalysis and chromatography (Liang et al. 2008).

To better help understand the behaviour of CNC particles in suspension, we studied the microhydration of relevant functional groups present on the surface of cellulose nanocrystals with and without the presence of an electrolyte (sodium) by means of high-level quantum chemical computations. The functional groups are primary alcohols, which are ubiquitous in cellulosic materials, carboxylates and sulphates. Such results will help design future classical simulation force fields and/or mesoscale force fields which are needed to tackle problems involving nanocellulose due the sheer size of these systems. Moreover, the results will also help better understand the effect of chemical modification occurring on the different nanocrystal surfaces as well as the behaviour of those particles towards water and electrolytes. The performance of recent DFT functionals at correctly reproducing key interactions is also assessed.

## Computational methods

The computation work in this manuscript was devised as follow. First, the accuracy of the several DFT functionals at reproducing interaction energies between different functional groups fragments and water or electrolyte was tested against higher level calculations. Once the DFT methods have been tested, the calculation of crystalline cellulose surfaces is performed using other, lower cost DFT methods because of the size of the systems. These methods are also tested against the higher level calculations described above. The adsorption energies of water and sodium is also computed using these DFT methods. Finally, the interaction energies between crystalline cellulose slabs is computed as well. The following sections describes in-depth the procedures and methods used (Scheme 1).

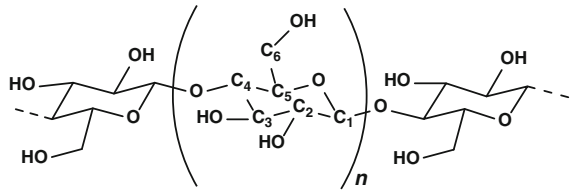


**Scheme 1** Structure of cellulose with atom numberings

### Benchmark potential energy curves

Potential energy curves between water and ethanol, carboxylate and methyl sulphate ester used as stand-ins for the functional groups found in native or modified cellulose were constructed to evaluate the behaviour of selected computation methods at properly reproducing the benchmark values near the equilibrium distance and also at longer ranges. The interaction energy between water and the surface moiety as a function of intermolecular distances was calculated and basis set superposition error (BSSE) was corrected using the counterpoise method (Boys and Bernardi 1970; Simon et al. 1996). The distances chosen between the hydroxyl oxygen and water oxygen for ethanol, and between the water oxygen and the central carbon and sulphur atoms for the carboxylate and sulphate ester groups were used for the potential energy curves. The interaction energies were also computed using the same distance criteria in the presence of a sodium ion with and without water. The systems used for the calculation of interaction energy are shown in Fig. 1. Relaxed potential energy scans (geometry optimization at each point on the curves) were done up to a distance of 10 Å. The interaction energies were calculated as followed:

$$\Delta E_{\text{interaction}} = E_{Total} - (E_{Fragment} + E_{H_2O}) \quad (1)$$

In the cases where there are three fragments present, the energy component $E_{\text{Fragment}}$ consists of the ion

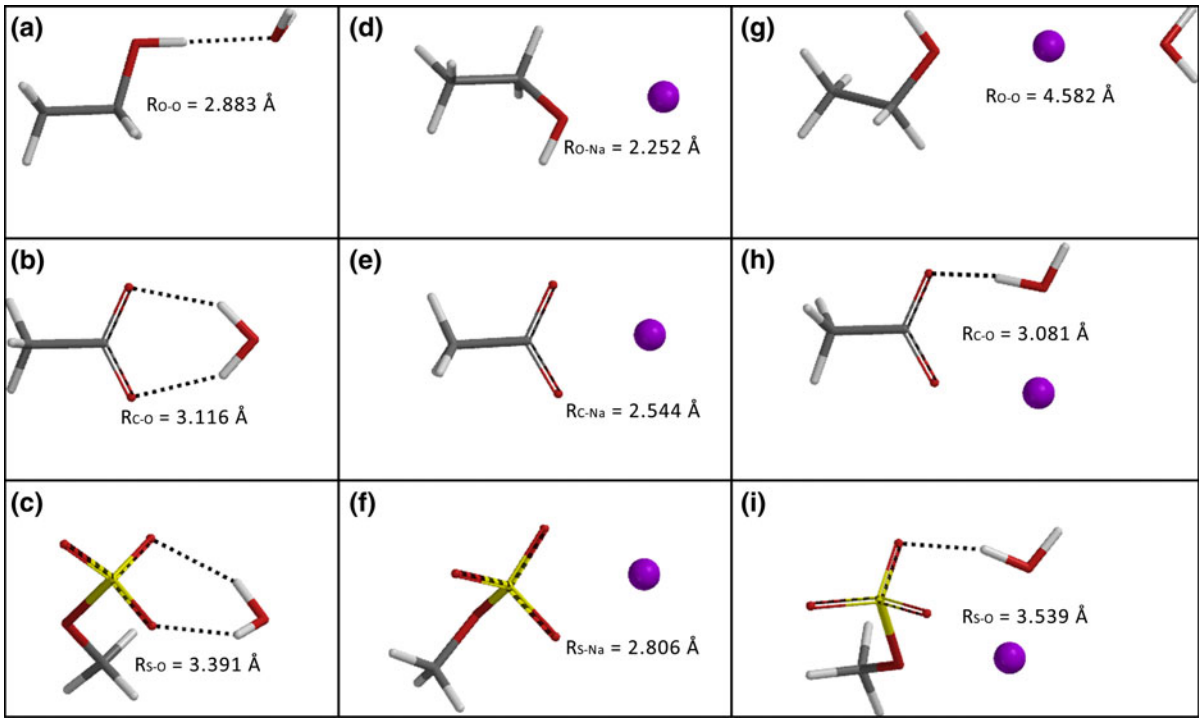


**Fig. 1** MP2/cc-pVTZ optimised geometries of the monohydrated complexes. Sodium ion is shown in *purple*

pair. All calculations were done in the gas phase with the Gaussian09 Rev. C.01 (Frisch et al. 2011) and Spartan 10 V1.1.0 (Shao et al. 2010) software.

Geometry optimizations were done at the MP2 level using Dunning's consistent correlated cc-pVTZ basis set, and the energies were evaluated with the aug-cc-pVTZ basis set (Dunning 1989) as benchmarks. MP2 calculations offer good accuracy for non-covalent interactions both for geometries and binding energies, especially for systems containing hydrogen bonds (Hobza 2011). The potential energy curves were also calculated using DFT methods. The B3LYP (Becke 1993; Lee et al. 1988), M06-2X (Zhao and Truhlar 2007) and the long-range dispersion corrected ωB97X-D (Chai and Head-Gordon 2008) functionals were also used with the 6-311++G** Pople basis set. DFT methods are much faster and scale better with system size than MP2 methods, hence the use of truncated systems. The accuracy of those less computationally intensive methods will be compared against MP2 results.

## Simulation of cellulose surfaces

Since the morphology of cellulose Iβ nanocrystals in aqueous dispersion has both the hydrophilic (1 1 0) and (1 −1 0) surfaces exposed to the solvent (Moon et al. 2011), those surfaces were studied. The surfaces were built using the known x-ray crystal structure and cleaving the proper planes (Nishiyama et al. 2002). The surfaces were optimised using both the solid state periodic DFT code CASTEP as implemented in the Materials Studio 6.0 package (Clark and Segall 2005) and wave function methods using Gaussian09. In the CASTEP calculations, the systems were optimized using the PBE functional (Perdew et al. 1996) with Grimme's dispersion correction scheme (Grimme 2006), as this method proved useful in predicting the crystal structure of cellulose I (Li et al. 2011). The energy cut-off for all periodic DFT calculations was 600 eV, and norm-conserving pseudopotentials were used. The system was built with 3 slabs of 2 cellulose chains with periodic boundary conditions along the chain axis, mimicking infinite chain length. Upon optimization of the surfaces, the adsorption energies of water, sodium and water-on-cellulose/sodium ion pairs were also calculated.

Calculations using wave function methods used the surfaces of 4 cellulose strands of 3 glucose molecules each arranged in the Iβ form. The B3LYP functional along with the 6-31G* basis set was used. Adsorption

energies of water, sodium and water-on-ion pairs were also computed at the same level of theory, using BSSE correction. Those interaction energies were also computed in implicit water using the IEFPCM solvation scheme (Scalmani and Frisch 2010). The implicitly solvated interaction energies were not BSSE corrected since the counterpoise method was not available with solvation.

### Cellulose surface–surface interaction energies

In order to better understand the interaction between CNC rods, the potential energy curves between the (1 1 0)—(1 1 0) and (1 −1 0)—(1 −1 0) surfaces were calculated at the B3LYP/6-31G* level of theory, using single point calculations only. The previously optimised surface fragments were placed on top, parallel to each other, and separated by distances from 9 to 25 Å. The effect of the molecular orientation was also studied by placing the cellulose clusters 10 Å apart, and then having the topmost surface rotated clockwise from 0 to 25 degrees, by increments of 5 degrees.

## Results and discussion

### Intermolecular interaction potentials between water: CNC functional groups

The single water hydration complex structures with ethanol, acetate and methyl sulphate are represented in Fig. 1a–c respectively. The interaction energies and the equilibrium distances computed using the MP2 and DFT methods are compiled in Table 1. The potential energy curves for the monohydrated complexes computed at various levels of theory are shown in Fig. 2. Calculations show the $R_{O–O}$ ethanol–water equilibrium distance at 2.883 Å at the MP2/cc-pVTZ geometry. This result is similar with a previous study (Fileti et al. 2004) which shows this distance at 2.914 Å at the MP2/aug-cc-pVDZ. These slight differences can be attributed to the use of diffuse functions in the augmented polarization of consistent basis sets. Intermolecular distances of hydrogen bonded complexes have been shown to be susceptible to the use of such augmented basis sets (Lane and Kjaergaard 2009). The counterpoise corrected interaction energy calculated at the MP2/aug-cc-pVTZ level is −19.0 kJ/mol, similar to the (Fileti et al. 2004) previous study where they obtained a value of −17.9 kJ/mol at the MP2/aug-cc-pVDZ level.

The binding energies and geometries were also calculated with DFT methods using a lighter, speedier basis set. As can be seen in Table 1, the equilibrium $R_{O–O}$ values for the B3LYP, M06-2X and ωB97X-D functionals are 2.914, 2.882 and 2.878 Å respectively. The M06-2X method reproduces best the MP2/cc-pVTZ intermolecular distance at a fraction of the computational cost. When it comes to the binding energies, B3LYP yields the best results with −19.3 kJ/mol. Both the M06-2X and ωB97X-D functionals lead to stronger binding energies then those obtained at the MP2/aug-cc-pVTZ levels. A recent study (Hirota et al. 2009) assessed the performance of various DFT

**Table 1** Equilibrium distances (Å) and interaction energies (kJ/mol) of the monohydrated complexes for the various computational methods used

| Complex | B3LYP/6-311++G** | | M06-2X/6-311++G** | | ωB97X-D/6-311++G** | | MP2/cc-pVTZ | | MP2/aug-cc-pVTZ |
|---|---|---|---|---|---|---|---|---|---|
| | $r_{eq}$ | ΔE | $r_{eq}$ | ΔE | $r_{eq}$ | ΔE | $r_{eq}$ | ΔE | ΔE |
| EtOH–$H_2O$ | 2.914 | −19.3 | 2.882 | −22.6 | 2.878 | −22.1 | 2.883 | −18.4 | −19.0 |
| EtOH–$Na^+$ | 2.192 | −119.6 | 2.181 | −121.0 | 2.212 | −115.5 | 2.252 | −109.7 | −108.3 |
| EtOH/$Na^+$–$H_2O$ | 4.458 | −90.5 | 4.418 | −93.4 | 4.494 | −87.7 | 4.582 | −84.1 | −81.1 |
| $CH_3COO^-$–$H_2O$ | 3.171 | −84.7 | 3.146 | −93.9 | 3.162 | −90.4 | 3.116 | −81.3 | −85.2 |
| $CH_3COO^-$–$Na^+$ | 2.506 | −413.9 | 2.480 | −479.2 | 2.524 | −604.3 | 2.544 | −482.2 | −595.2 |
| $CH_3COO^-$/$Na^+$–$H_2O$ | 3.101 | −130.8 | 3.045 | −146.9 | 3.096 | −133.2 | 3.081 | −125.2 | −124.8 |
| $CH_3OSO_3^-$–$H_2O$ | 3.484 | −59.4 | 3.393 | −72.1 | 3.428 | −67.2 | 3.391 | −59.1 | −63.0 |
| $CH_3OSO_3^-$–$Na^+$ | 2.747 | −465.7 | 2.721 | −537.3 | 2.765 | −536.7 | 2.806 | −621.7 | −525.4 |
| $CH_3OSO_3^-$/$Na^+$–$H_2O$ | 3.568 | −92.3 | 3.533 | −102.4 | 3.554 | −98.2 | 3.539 | −90.5 | −90.0 |

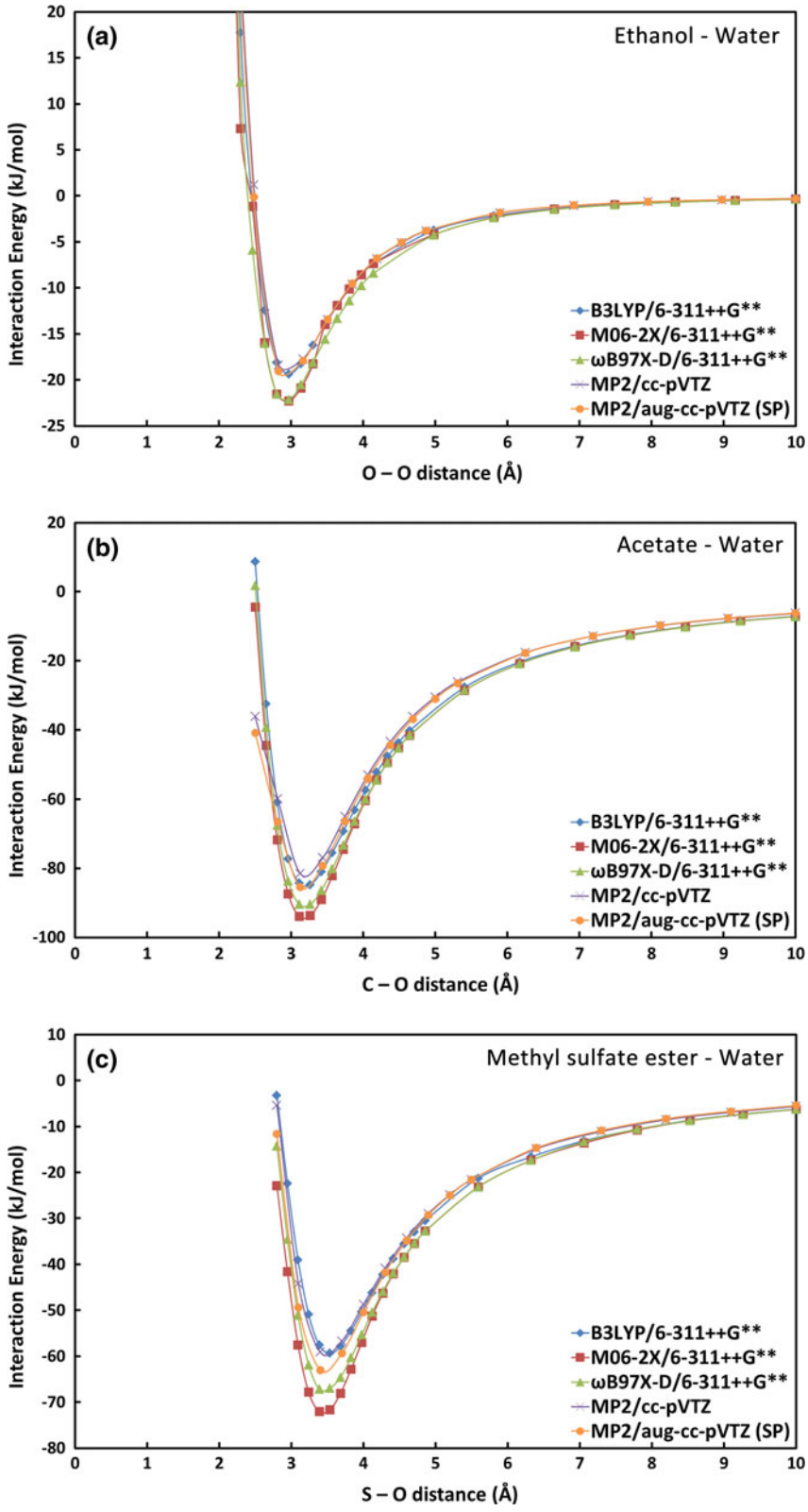


**Fig. 2** Potential energy curves of the monohydrated complexes

functionals for the prediction of binding energies of water clusters, and it also concluded that B3LYP outperforms the M06-2X functional. ωB97X-D yields less accurate results for the interaction energy.

Water binding to an acetate molecule was investigated. In this case, the acetate moiety mimics the carboxylate groups on the surface of the CNC. The MP2/cc-pVTZ optimised intermolecular distance obtained is 3.116 Å. The counterpoised corrected MP2/aug-cc-pVTZ interaction energy (−85.2 kJ/mol) is in good agreement with another study (Řezáč and Hobza 2012) which evaluated this binding energy at −88.1 kJ/mol at the CCSD(T)/CBS level of theory. It can be seen from Table 1 and Fig. 2 that all DFT methods yield higher intermolecular distances, with the M06-2X functional being the closest to the MP2 computed value. As was the case with the ethanol–water complex, the popular B3LYP function gives the best accuracy in regards to the binding energy with an error of only 0.5 kJ/mol against the highest level of theory used in this study. Other functionals overestimate this interaction energy by 8.7 kJ/mol (M06-2X) and 5.2 kJ/mol (ωB97X-D).

Sulphate ester groups are also common CNC surface modifications. The intermolecular potential curves are shown in Fig. 2. Given the results compiled in Table 1, the M06-2X functional gives the best geometrical results (3.393 vs. 3.391 Å) while B3LYP still gives the best interaction energy estimates with an error of only 3.6 kJ/mol. The next closest functional is the long-range dispersion corrected ωB97X-D, which gives an error of −4.2 kJ/mol. Overall, for both neutral and negatively charged hydration complexes, B3LYP performs well for energetics while Truhlar's M06-2X gives accurate geometrical parameters. The computed interaction energies show that water has greater affinity to the carboxylate group than the methyl sulphate group and finally the primary alcohol. CNC suspensions are usually easier made with negatively charged nanoparticles (Lu and Hsieh 2010).

## Interaction potentials between the sodium ion and CNC surface groups

The interaction potentials between the sodium ion and the cellulose nanocrystal surface functionalities were evaluated. The equilibrium distances and interaction energies can be seen in Table 1 and the structures are shown in Fig. 1d–f. Sodium ion shows great affinity with both the carboxylate (−595.2 kJ/mol) and the sulphate group (−525.4 kJ/mol) at equilibrium distances of 2.544 and 2.806 Å respectively, as is expected of anion–cation interactions. Sodium ion also has affinity for primary alcohols; the binding energy between the ion and ethanol is −108.3 kJ/mol which is typical for cation–dipole non-covalent interactions (Atkins and Paula 2006). There are some noticeable differences between the interaction energies computed with the cc-pVTZ and aug-cc-pVTZ basis sets, especially with the negatively charged molecules. This indicates the importance in using diffuse basis functions when treating such ionic interactions. The interaction energies of the $Na^+$ ion with functional groups present on the crystal surface are more than fivefold the binding energy for water. This seems to indicate that adsorption of sodium on CNC surfaces is likely.

Figure 3 shows the potential energy curves computed at the various theory levels. In the anion–cation interactions, some energy curves computed by DFT functionals show unexpected variations at longer distances. This is the case with the B3LYP and M06-2X functionals. This raises doubts on the reliability of those functionals to properly evaluate the behaviour of such interactions at longer range. Even more so, the B3LYP and M06-2X functionals show large errors on the interaction energies. Compared to the MP2/aug-cc-pVTZ values, B3LYP underestimates the binding energy by more than 30 percent while M06-2X does so by 19.5 %. The ωB97X-D functional gives the best results for both the interaction energies and the intermolecular distances for all complexes. It also better reproduces the MP2/aug-cc-pVTZ curves at longer distances, implying that among the tested functionals, it is the best choice for strictly anionic interactions.

## Effect of the sodium ion on the water potential energy curves

Energy curves between the various nanocrystalline functional group ion pairs and water are shown in Fig. 4. The global minimum complexes are shown in Fig. 1g–i. The geometry of the complexes seem to indicate that there are cooperative interactions with both the sodium ion and the CNC surface groups. On the carboxylate and sulphate groups, water interacts with both hydrogen bonding and cation–dipole

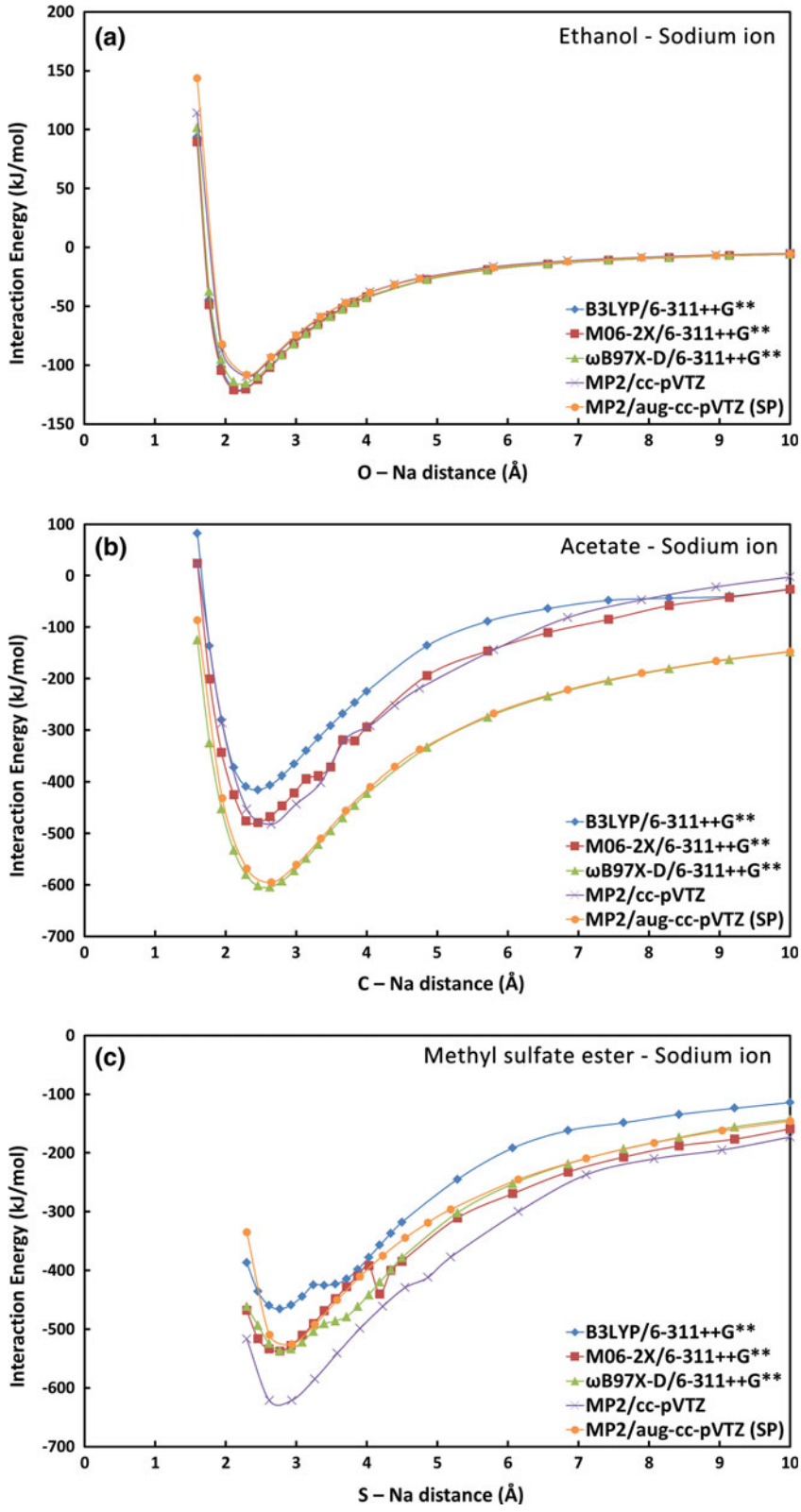


**Fig. 3** CNC functional groups interaction potentials with sodium ion

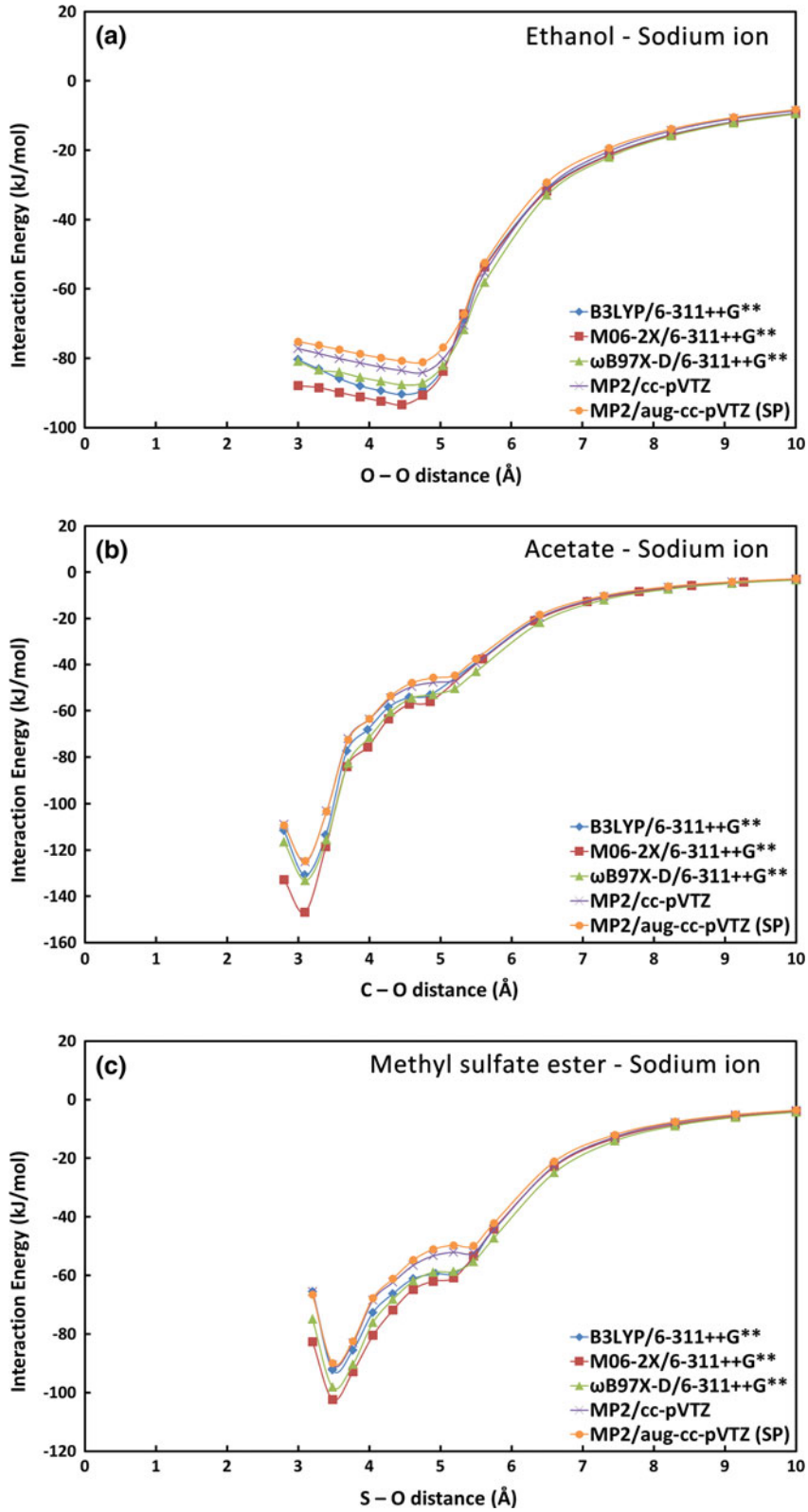


**Fig. 4** Potential energy curves of the monohydrated complexes with sodium

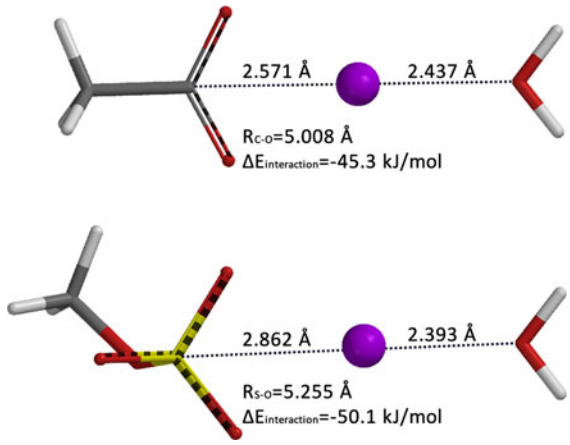


**Fig. 5** MP2/cc-pVTZ optimised structures and geometrical parameters of the second minimum configurations

interactions through the oxygen lone pairs. Indeed, the stronger calculated interaction energies over the single water hydration complexes support this claim. The interaction energy of water with the carboxylate/sodium ion pair is −124.8 kJ/mol at the MP2/aug-cc-pVTZ level. The value is −90.0 kJ/mol for the sulphate group. The interaction energy of water with the ethanol/sodium pair is also higher with a value of −81.1 kJ/mol. The B3LYP and ωB97X-D both give good results for the interactions energies with B3LYP being slightly superior with an average relative error of 6.3 % while ωB97X-D overestimates the binding energy by 8.0 %. The M06-2X functional is clearly the worst at reproducing the MP2 interaction energies of such complexes with an error of 15.6 %. The ωB97X-D functional also predicts best the equilibrium geometries.

Interestingly, with the inclusion of a sodium ion, the potential energy curves (Fig. 4) of the carboxylate and sulphate groups show a second local minimum at around 5 Å. The MP2/cc-pVTZ geometries and aug-cc-pVTZ binding energies of those complexes are shown in Fig. 5. The C–O and S–O equilibrium distances in those structures are quite similar (5.008 and 5.255 Å respectively). In these configurations, water no longer interacts with both components of the ion pair but rather with sodium only in a "sandwich" type structure, much like the one found with ethanol. The inclusion of modified CNC surface groups creates different types of hydration complexes around them upon the addition of sodium chloride, which showcases the affinity of both the sodium cation and water towards cellulosic materials.

## DFT optimised cellulose surface structures

Very few studies have been done on crystalline cellulose at the quantum level until recently. Other than the prediction of the crystal structure of cellulose I using DFT methods (Li et al. 2011), the vibrational spectra of polysaccharide clusters was predicted using the B3LYP functional (Barsberg 2010). Moreover, a benchmark study testing the ability of various DFT functionals at reproducing the most stable conformations of several carbohydrates, including *β*-D-glucopyranose, has been done previously (Csonka et al. 2009). Unfortunately, the calculations were limited to carbohydrates in vacuum therefore neglecting crystal structure effects. Nevertheless, their calculations shows that the PBE structures are in good agreement with reference MP2 calculations made on the same structures. Other than that, insight has been gathered on the stacking of cellulose chains via hydrogen bonding and dispersive interactions using cellobiose units as input models with the M06-2X functional (Parthasarathi et al. 2011). However, to the best of our knowledge, no studies were carried out on modified cellulose surfaces. The optimized structures of the cellulose surfaces using both the PBE-D and B3LYP functionals are similar. The PBE-D structures, along with the electrostatic potential maps of the surfaces are shown in Fig. 6. The optimised unmodified surface shows a $O_3 \cdots O_5$ hydrogen bond which is consistent with the crystal structure and previous computational work as well (French et al. 2013). The most striking effect of the carboxylate and sulphate ester chemical modifications is the overall more negative potential energy surface, which is to be expected. We also find the *gt* conformations of the $C_6$ hydroxymethyl group are the most stable, which is consistent with experimental NMR data, hence the lack of intermolecular $O_6 \cdots O_2$ hydrogen bonds (Isogai et al. 1989). Moreover, the $O_3 \cdots O_5$ intrachain hydrogen bond is broken as $O_3$ now acts as a donor to carboxylate oxygen, although this interaction is rather weak. We also find the $O_2$ hydrogen interacts with the other oxygen atom. In the case of the sulphated surface, we find again that the $O_3$ acts as a hydrogen bonding donor to one of the sulphate oxygens. However, the geometry of the surface does not allow $O_2$ to form hydrogen bonds. We

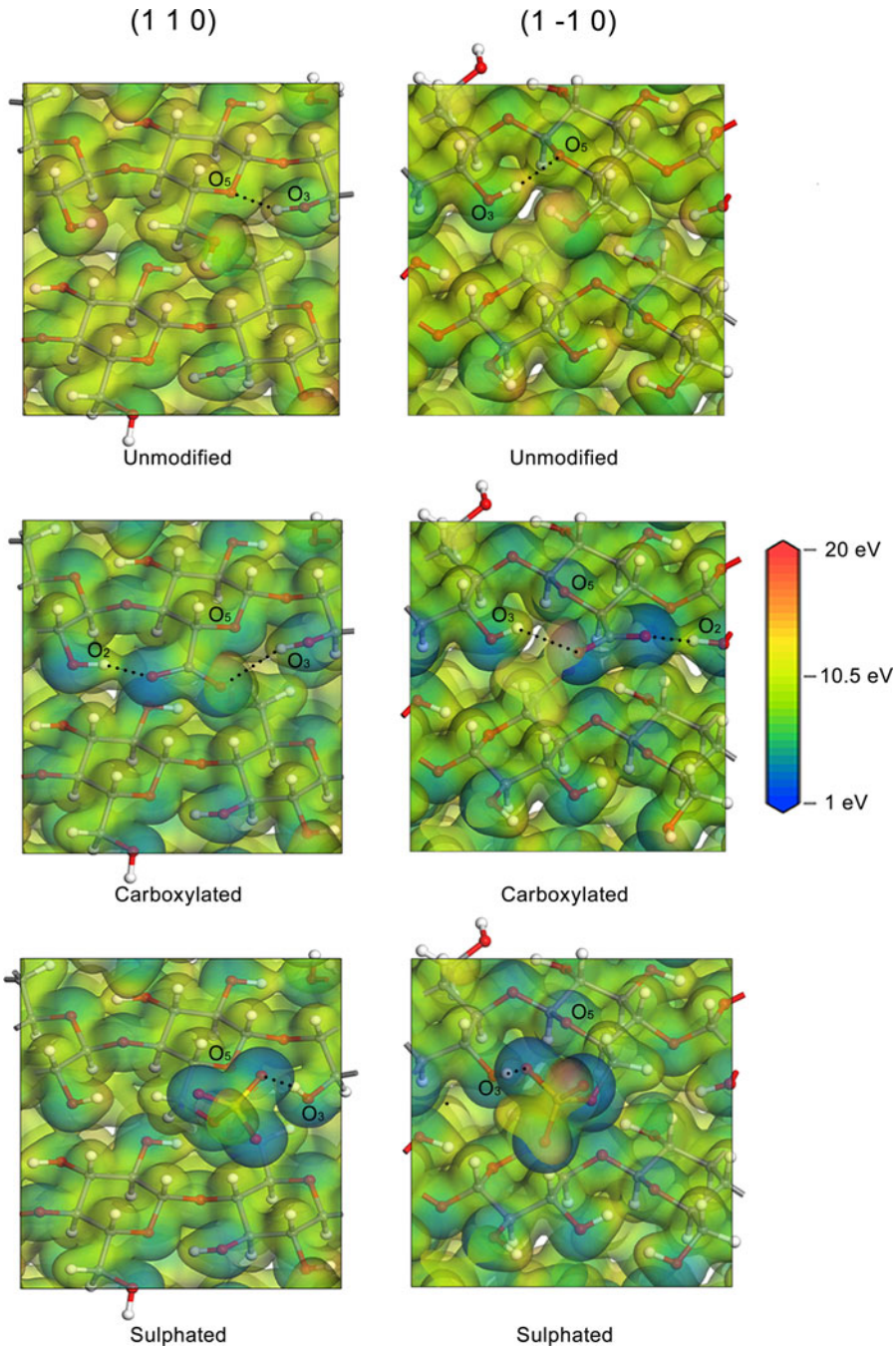


**Fig. 6** Optimised PBE-D structure of the cellulose surfaces along with the electrostatic potential maps. Note the $O_3 \cdots O_5$ hydrogen bonds

find very similar geometries between the (1 1 0) and (1 −1 0) surfaces, and only the topmost surface layers showed structural changes. However, upon inspection of the electrostatic potential maps, we find the (1 −1 0) carboxylated and sulphated surfaces to be slightly more negative than their (1 1 0) counterparts.

## Adsorption of water and sodium ion on the cellulose surfaces

The adsorption of water and sodium cation on the pristine and modified cellulose (1 1 0) and (1 −1 0) surfaces was calculated at the PBE-D and B3LYP/

**Table 2** Benchmarking of the PBE-D and B3LYP/6-31G* methods equilibrium distances (Å) and interaction energies (kJ/mol) of water and sodium with the small model fragments and adsorption energies with the (1 1 0) cellulose surfaces

| Cellulose Surface | PBE-D (Benchmark models) | | B3LYP/6-31G* (Benchmark models) | | PBE-D | | B3LYP/6-31G* | | B3LYP/6-31G* (solvated in water) |
|---|---|---|---|---|---|---|---|---|---|
| | $r_{eq}$ | ΔE | $r_{eq}$ | ΔE | $r_{eq}$ | ΔE | $r_{eq}$ | ΔE | ΔE |
| Unmodified—$H_2O$ | 2.910 | −21.9 | 2.859 | −23.1 | 2.782 | −76.6 | 2.765 | −65.6 | −67.4 |
| Unmodified—$Na^+$ | 2.199 | −122.1 | 2.172 | −126.4 | 2.506 | −608.0 | 3.887 | −356.3 | −73.9 |
| Unmodified/$Na^+$–$H_2O$ | 4.510 | −87.8 | 4.360 | −100.9 | 3.561 | −79.4 | 3.768 | −110.3 | −81.4 |
| Carboxylated—$H_2O$ | 3.162 | −90.6 | 3.136 | −88.3 | 3.316 | −71.3 | 3.398 | −90.8 | −87.4 |
| Carboxylated—$Na^+$ | 2.524 | −497.6 | 2.544 | −395.7 | 2.724 | −854.1 | 2.663 | −649.5 | −124.8 |
| Carboxylated/$Na^+$–$H_2O$ | 3.638 | −86.3 | 3.690 | −79.0 | 3.694 | −76.0 | 3.562 | −64.5 | −84.1 |
| Sulphated—$H_2O$ | 3.406 | −66.1 | 3.403 | −56.7 | 3.415 | −53.9 | 3.479 | −42.0 | −26.7 |
| Sulphated—$Na^+$ | 2.760 | −427.9 | 2.719 | −450.7 | 2.921 | −910.1 | 2.829 | −652.0 | −113.7 |
| Sulphated/$Na^+$–$H_2O$ | 3.641 | −81.7 | 3.610 | −77.5 | 4.094 | −76.1 | 3.903 | −77.4 | −62.7 |

The distance criteria for the cellulose surface and the water/sodium ion components are the same as those in the benchmark calculations

6–31G* levels. The size of the systems made the use of the more complete 6-311++G** basis set impossible and thus, the PBE-D and B3LYP methods were also benchmarked using the same models as previously indicated. The calculation of the PBE-D interaction energies of water with ethanol, acetate and the methyl sulphate ester fragments are shown in Table 2. Those energies vary by −2.9, −5.4 and −3.1 kJ/mol respectively compared to the higher level MP2/aug-cc-pVTZ calculations. This shows that this function slightly overestimates the binding energies with water. The optimized distances are also found to be lower than the MP2 ones, by 0.027, 0.046 and 0.015 Å. Similar results are found using the B3LYP/6–31G*. It is found that this method overestimates the interaction energy of water with ethanol and acetate by 4.1 and 3.1 kJ/mol. The interaction of water with the methyl sulphate ester is found to be underestimated by 6.3 kJ/mol. These results seem to indicate that those methods show rather small errors in order to enable the computation of larger, more realistic cellulosic surfaces. However, the calculations involving the sodium cation seems to be less reliable at those levels of theory since compared to the MP2/aug-cc-pVTZ calculations, the energies can be underestimated by values up to 33 %(Acetate–$Na^+$) and also overestimated by 16.7 % (EtOH–$Na^+$). Those methods also seem to show large errors for the systems involving sodium and water, especially in the cases of the acetate and methyl sulphate ester moieties. Errors in the computed energies are found to be as large as −34.5 % for the acetate molecule and −13.9 % for the methyl sulphate ester. In conclusion, the benchmarking of the PBE-D and B3LYP/6–31G* level methods show decent ability to reproduce the interaction energies and geometries of water complexed with the fragmented functional groups. It seems larger basis sets/high levels of theory are useful with systems involving mixed ionic/electrostatic interactions.

The geometries of the (1 1 0) and (1 −1 0) surfaces with adsorbed water and sodium ion were optimized with the PBE-D and B3LYP/6–31G* level methods. The structures of the B3LYP/6–31G* (1 1 0) surfaces are shown in Fig. 7 and the adsorption energies in Table 2. The PBE-D and B3LYP (1 1 0) and (1 −1 0) surfaces show strong similarities when it comes to the conformations of adsorbates. First, the adsorption energy of water with the unmodified cellulose (1 1 0) surface is found to be much higher than the benchmark calculations, in both the PBE-D and B3LYP models. Upon inspection of the optimized structure in Fig. 7a, we found that the water molecule forms hydrogen bonds with two sites, which is not possible to observe in the models used in the benchmark calculations. The B3LYP/6–31G* absorption energies of water with the carboxylated surface is close to the MP2/aug-cc-pVTZ which indicates benchmark models can be accurate. However, the adsorption energy of water to the sulphated surface is lower than the benchmark models, which can be attributed by the discrepancies between the benchmark models and the more realistic surface models.

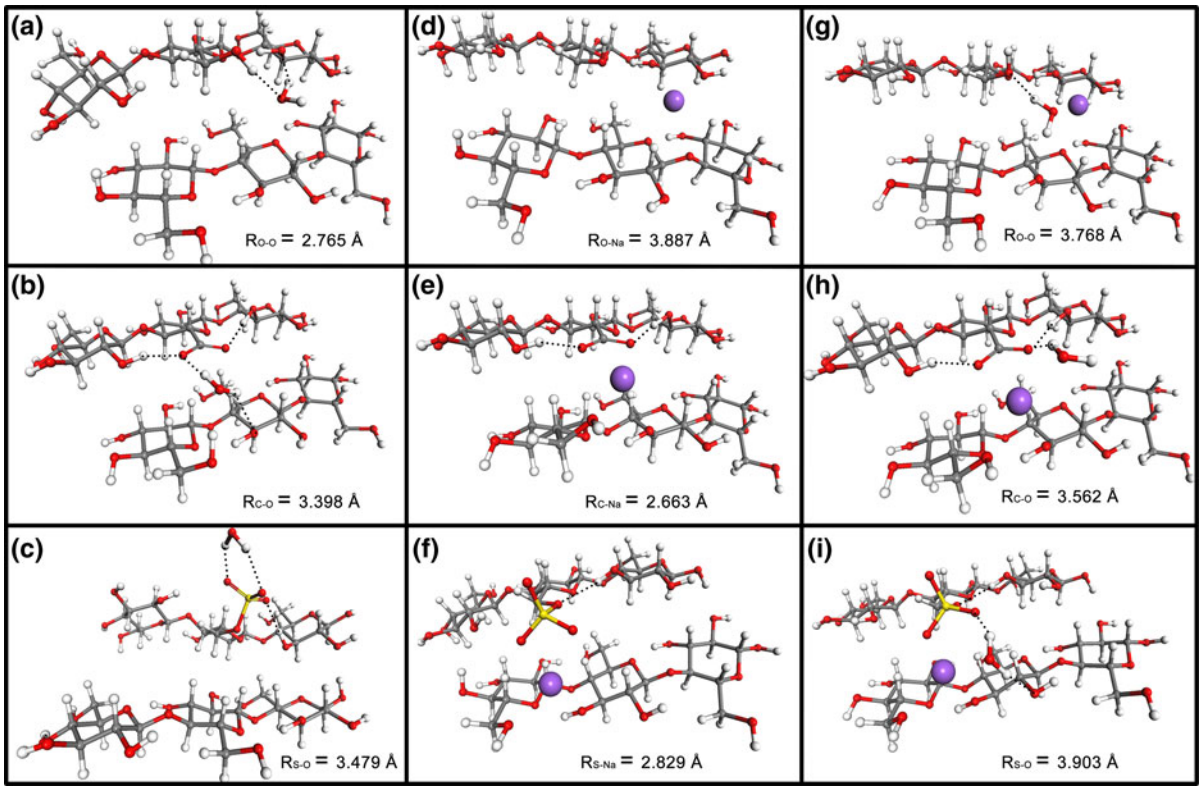


**Fig. 7** B3LYP/6–31G* optimised (1 1 0) cellulose surfaces with adsorbed water and sodium cation. The bottom cellulose layers are omitted for clarity. Only **a** still retains the $O_3 \cdots O_5$ intramolecular hydrogen bond

The adsorption energies of the sodium cation on the (1 1 0) surface are also found to be much higher than those calculated with the benchmark models. Looking at the structures shown in Fig. 7d–f, we find that the sodium interacts with multiple oxygen atoms on the surface, in similar fashion to experimental structures found previously by a joint experimental and theoretical study (Peralta-Inga et al. 2002). The very high interaction energies show that the cation has very strong affinity toward crystalline cellulosic surfaces—more than water. When calculating surfaces with both sodium and water molecules present, we find conformations in which water interacts with both the surface and the sodium cation in a similar fashion as the benchmark complexes. Those structures are shown in Fig. 7g–i. The adsorption of water with surfaces containing sodium is found to be higher with the unmodified and sulphated surface (−110.3 and −77.4 kJ/mol at the B3LYP/6–31G* level) than the surfaces without sodium. Water binds more weakly to the carboxylated/$Na^+$ surface. This shows the inclusion of sodium ions on the surface of cellulose can tune its hydrophilicity.

Adsorption of water and ions were calculated on the (1 −1 0) surface. The interaction energies are reported in Table 3. The adsorption energies of water to the surfaces are found to be slightly higher in all three cases. The same can be said for the adsorption of sodium cation. Water and ions thus interact differently with the different facets of cellulose crystals, which may help explain the previously observed anisotropic behaviour (Holt et al. 2010; Beck-Candanedo et al. 2006; Dong and Gray 1997).

The absorption energies were also calculated with implicit solvation in water to obtain more realistic energetic values, especially with the sodium cation. In the gas phase, sodium adsorption on cellulosic surfaces has interaction energies even higher than some covalent bonds (Atkins and Paula 2006). The calculation of adsorption energies with implicit water with the B3LYP functional of water with both the (1 1 0) and (1 −1 0) surfaces only changes by a few kJ/mol. However, in the systems containing sodium, the interaction energies are significantly lower with values corresponding to typical non-covalent interactions.

**Table 3** Equilibrium distances (Å) and interaction energies (kJ/mol) of water and sodium with the (1 −1.0) cellulose surface. The distance criteria are the same as those in the benchmark calculations

| Cellulose surface | PBE-D | | B3LYP/6-31G* | | B3LYP/6-31G* (solvated in water) |
|---|---|---|---|---|---|
| | $r_{eq}$ | ΔE | $r_{eq}$ | ΔE | ΔE |
| Unmodified—$H_2O$ | 2.758 | −66.2 | 7.761 | −71.4 | −77.9 |
| Unmodified—$Na^+$ | 2.382 | −577.6 | 3.464 | −351.2 | −65.7 |
| Unmodified/$Na^+$–$H_2O$ | 4.211 | −80.4 | 4.284 | −106.9 | −77.7 |
| Carboxylated—$H_2O$ | 3.195 | −73.8 | 3.233 | −91.5 | −87.4 |
| Carboxylated—$Na^+$ | 2.609 | −973.8 | 2.603 | −732.9 | −157.2 |
| Carboxylated/$Na^+$–$H_2O$ | 3.822 | −74.3 | 3.581 | −91.5 | −73.8 |
| Sulphated—$H_2O$ | 3.442 | −52.1 | 3.555 | −64.6 | −59.9 |
| Sulphated–$Na^+$ | 2.911 | −956.6 | 2.868 | −689.2 | −103.6 |
| Sulphated/$Na^+$–$H_2O$ | 3.421 | −100.2 | 3.492 | −102.1 | −83.2 |

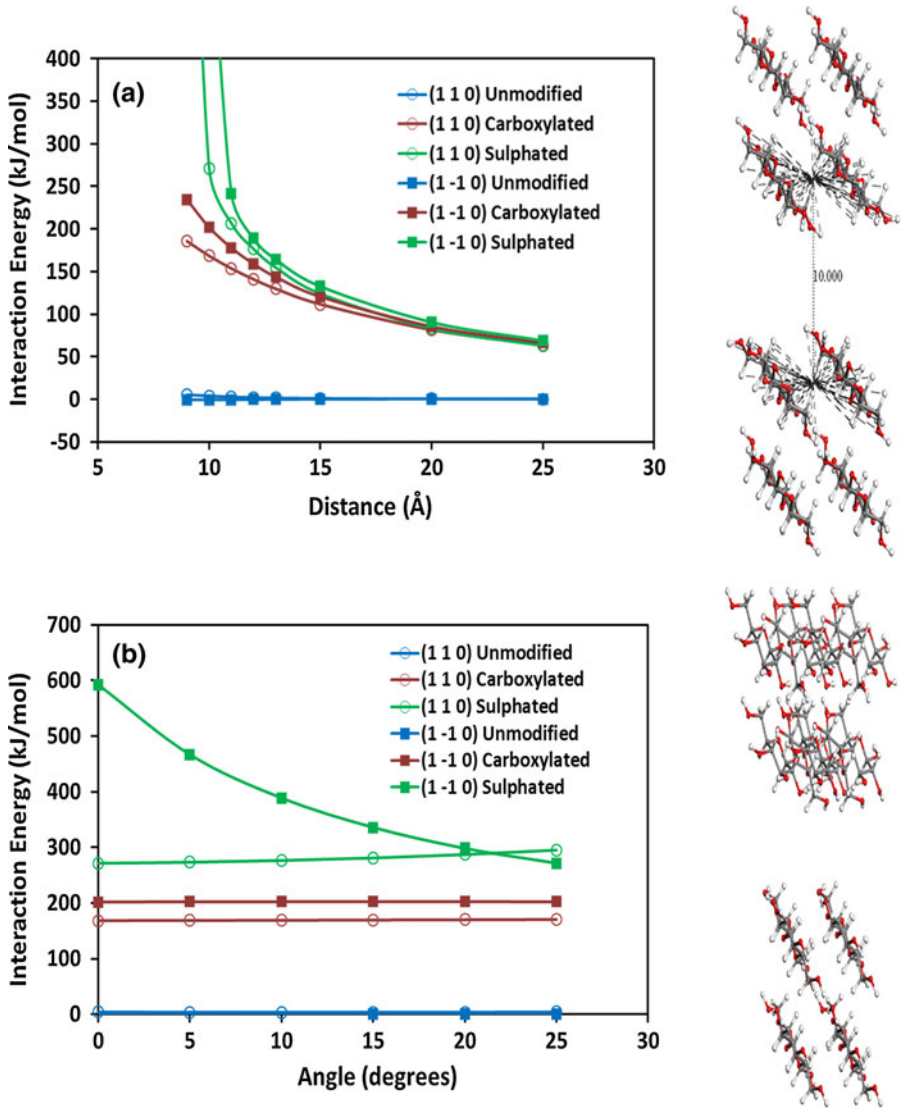


**Fig. 8** Interaction energies between cellulose surfaces: **a** the curves as function of the distance between the surfaces and **b** the curves as function of the angle between the surfaces

Even with the solvation scheme, it is still found that sodium adsorption on the crystal surface is likely, even in the case of the neutral, unmodified surface.

### Potential energy curves for cellulose surface–surface interaction

Interaction energy curves between two cellulose (1 1 0) and two cellulose (1 −1 0) surfaces were calculated as a function of distance and angles between them at the B3LYP/6–31G* level of theory. The results are shown in Fig. 8. The unmodified surfaces show little to no repulsion between each other which is to be expected since pristine CNCs are difficult to disperse. Sulphated surfaces show the strongest repulsions. The results also show, the (1 −1 0) surfaces show stronger repulsion towards each other which could lead us to believe that CNCs self-assemble by stacking (1 1 0) surfaces. Moreover, the energy curves were also calculated by varying the angle between the cellulosic clusters. The curves in Fig. 8b show that the repulsion strength of (1 −1 0) sulphated surfaces decreases when the surfaces are rotated away from each other while it very slightly increases in the case of the (1 1 0) surface. This could indicate that the chiral nematic behaviour of CNC suspensions are not only caused by chiral twists in cellulose found in a previous computational study (Paavilainen et al. 2011) but also by the crystals simply rotating away from each other in order to minimize the repulsion energy.

## Conclusions

The study of monohydrated hydration complexes reveals the performance of three DFT functionals at reproducing higher level MP2 results. B3LYP was found to correctly reproduce the potential energy curves of single water complexes with ethanol, acetate and methyl sulphate. When dealing with strictly ionic interactions, the long-range dispersion corrected functional ωB97X-D best reproduced the MP2 results. For complexes with both water and sodium, the B3LYP and ωB97X-D functionals both yield satisfactory results.

The PBE-D and B3LYP/6–31G* methods were also benchmarked and were found to correctly reproduce the interaction energies with water. Unmodified, carboxylated and sulphated cellulose surfaces were optimized using the B3LYP and PBE-D functionals, and it was found that the (1 −1 0) surface has a slightly more negative electrostatic potential map. Both surfaces show strong affinity toward water and sodium cations. The adsorption energies are found to be slightly higher on the (1 −1 0) surface. The introduction of negatively charged groups on the surfaces also showed hydrogen bond network changes. Potential energy curves between cellulose surfaces were also calculated. The results showed that the (1 −1 0) surfaces were more repulsive toward each other than the (1 1 0) surfaces. Those results can help better understand the self-assembly mechanism of CNCs in order to accelerate development of novel materials based on natural resources.

**Acknowledgments** We thank NSERC (National Sciences and Engineering Research Council of Canada), ArboraNano and FRQNT (Fonds de Recherche du Québec–Nature et Technologies) for financial support. We thank the Compute Canada network and Calcul Québec for their computational resources. We also thank FPInnovations.



## References

Asefa T (2012) Chiral nematic mesoporous carbons from self-assembled nanocrystalline cellulose. Angew Chem Int Ed Engl 51:2008–2010. doi:10.1002/anie.201107332

Atkins P, Paula Jd (2006) Physical chemistry. W. H Freeman, New York

Barsberg S (2010) Prediction of vibrational spectra of polysaccharides—simulated IR spectrum of cellulose based on density functional theory (DFT). J Phys Chem B 114:11703–11708. doi:10.1021/jp104213z

Beck S, Bouchard J, Berry R (2010) Controlling the reflection wavelength of iridescent solid films of nanocrystalline cellulose. Biomacromolecules 12:167–172. doi:10.1021/bm1010905

Beck S, Bouchard J, Berry R (2012) Dispersibility in water of dried nanocrystalline cellulose. Biomacromolecules 13:1486–1494. doi:10.1021/bm300191k

Beck-Candanedo S, Roman M, Gray DG (2005) Effect of reaction conditions on the properties and behavior of wood cellulose nanocrystal suspensions. Biomacromolecules 6:1048–1054. doi:10.1021/bm049300p

Beck-Candanedo S, Viet D, Gray D (2006) Induced phase separation in cellulose nanocrystal suspensions containing ionic dye species. Cellulose 13:629–635. doi:10.1007/s10570-006-9084-x

Becke AD (1993) Density-functional thermochemistry. III. The role of exact exchange. J Chem Phys 98(7):5648–5652. doi:10.1063/1.464913

Boys SF, Bernardi F (1970) The calculation of small molecular interactions by the differences of separate total energies. Some procedures with reduced errors. Mol Phys 19(4): 553–566. doi:10.1080/00268977000101561

Chai J-D, Head-Gordon M (2008) Long-range corrected hybrid density functionals with damped atom-atom dispersion corrections. Phys Chem Chem Phys 10:6615–6620. doi:10.1039/b810189b

Clark S, Segall M (2005) First principles methods using CASTEP. Z Kristallogr 220:567–570. doi:10.1524/zkri.220.5.567.65075

Dong XM, Gray DG (1997) Effect of counterions on ordered phase formation in suspensions of charged rodlike cellulose crystallites. Langmuir 13:2404–2409. doi:10.1021/la960724h

Dong XM, Kimura T, Revol J-F, Gray DG (1996) Effects of ionic strength on the isotropic: chiral nematic phase transition of suspensions of cellulose crystallites. Langmuir 12:2076–2082. doi:10.1021/la950133b

Dunning TH (1989) Gaussian basis sets for use in correlated molecular calculations. I. The atoms boron through neon and hydrogen. J Chem Phys 90:1007–1023. doi:10.1063/1.456153

Eichhorn SJ (2011) Cellulose nanowhiskers: promising materials for advanced applications. Soft Matter 7:303–315. doi:10.1039/C0SM00142B

Elazzouzi-Hafraoui S, Nishiyama Y, Putaux J-L, Heux L, Dubreuil F, Rochas C (2007) The shape and size distribution of crystalline nanoparticles prepared by acid hydrolysis of native cellulose. Biomacromolecules 9:57–65. doi:10.1021/bm700769p

Fileti EE, Chaudhuri P, Canuto S (2004) Relative strength of hydrogen bond interaction in alcohol–water complexes. Chem Phys Lett 400:494–499. doi:10.1016/j.cplett.2004.10.149

French A, Concha M, Dowd M, Stevens E (2013) Electron (charge) density studies of cellulose models. Cellulose: 1–13. doi:10.1007/s10570-013-0042-0

Frisch MJ, Trucks GW, Schlegel HB, Scuseria GE, Robb MA, Cheeseman JR, Scalmani G, Barone V, Mennucci B, Petersson GA, Nakatsuji H, Caricato M, Li X, Hratchian HP, Izmaylov AF, Bloino J, Zheng G, Sonnenberg JL, Hada M, Ehara M, Toyota K, Fukuda R, Hasegawa J, Ishida M, Nakajima T, Honda Y, Kitao O, Nakai H, Vreven T, Montgomery JA, Peralta JE, Ogliaro F, Bearpark M, Heyd JJ, Brothers E, Kudin KN, Staroverov VN, Kobayashi R, Normand J, Raghavachari K, Rendell A, Burant JC, Iyengar SS, Tomasi J, Cossi M, Rega N, Millam JM, Klene M, Knox JE, Cross JB, Bakken V, Adamo C, Jaramillo J, Gomperts R, Stratmann RE, Yazyev O, Austin AJ, Cammi R, Pomelli C, Ochterski JW, Martin RL, Morokuma K, Zakrzewski VG, Voth GA, Salvador P, Dannenberg JJ, Dapprich S, Daniels AD, Farkas, Foresman JB, Ortiz JV, Cioslowski J, Fox DJ (2011) Gaussian 09, Revision C.01. http://www.gaussian.com/g_tech/g_ur/m_citation.htm

GbI Csonka, French AD, Johnson GP, Stortz CA (2009) Evaluation of density functionals and basis sets for carbohydrates. J Chem Theory Comput 5(4):679–692. doi:10.1021/ct8004479

Grimme S (2006) Semiempirical GGA-type density functional constructed with a long-range dispersion correction. J Comput Chem 27:1787–1799. doi:10.1002/jcc.20495

Habibi Y, Lucia LA, Rojas OJ (2010) Cellulose nanocrystals: chemistry, self-assembly, and applications. Chem Rev 110:3479–3500. doi:10.1021/cr900339w

Hirota M, Tamura N, Saito T, Isogai A (2009) Surface carboxylation of porous regenerated cellulose beads by 4-acetamide-TEMPO/NaClO/NaClO system. Cellulose 16:841–851. doi:10.1007/s10570-009-9296-y

Hobza P (2011) The calculation of intermolecular interaction energies. Annu Rep Prog Chem Sect C 107:148–168. doi:10.1039/c1pc90005f

Holt BL, Stoyanov SD, Pelan E, Paunov VN (2010) Novel anisotropic materials from functionalised colloidal cellulose and cellulose derivatives. J Mater Chem 20:10058–10070. doi:10.1039/C0JM01022G

Isogai A, Usuda M, Kato T, Uryu T, Atalla RH (1989) Solid-state CP/MAS carbon-13 NMR study of cellulose polymorphs. Macromolecules 22:3168–3172. doi:10.1021/ma00197a045

Klemm D, Kramer F, Moritz S, Lindström T, Ankerfors M, Gray D, Dorris A (2011) Nanocelluloses: a new family of nature-based materials. Angew Chem Int Ed Engl 50:5438–5466. doi:10.1002/anie.201001273

Lane JR, Kjaergaard HG (2009) Explicitly correlated intermolecular distances and interaction energies of hydrogen bonded complexes. J Chem Phys 131:034307. doi:10.1063/1.3159672

Lee C, Yang W, Parr RG (1988) Development of the Colle-Salvetti correlation-energy formula into a functional of the electron density. Phys Rev B 37(2):785–789. doi:10.1103/PhysRevB.37.785

Li Y, Lin M, Davenport JW (2011) Ab Initio Studies of Cellulose I: crystal Structure, Intermolecular Forces, and Interactions with Water. J Phys Chem C 115:11533–11539. doi:10.1021/jp2006759

Liang C, Li Z, Dai S (2008) Mesoporous carbon materials: synthesis and modification. Angew Chem 47:3696–3717. doi:10.1002/anie.200702046

Liu D, Chen X, Yue Y, Chen M, Wu Q (2011) Structure and rheology of nanocrystalline cellulose. Carbohydr Polym 84:316–322. doi:10.1016/j.carbpol.2010.11.039

Lu P, Hsieh Y-L (2010) Preparation and properties of cellulose nanocrystals: rods, spheres, and network. Carbohydr Polym 82:329–336. doi:10.1016/j.carbpol.2010.04.073

Montanari S, Roumani M, Heux L (2005) Topochemistry of carboxylated cellulose nanocrystals resulting from TEMPO-mediated oxidation. Macromolecules 38:1665–1671. doi:10.1021/ma048396c

Moon RJ, Martini A, Nairn J, Simonsen J, Youngblood J (2011) Cellulose nanomaterials review: structure, properties and nanocomposites. Chem Soc Rev 40:3941–3994. doi:10.1039/C0CS00108B

Nishiyama Y, Langan P, Chanzy H (2002) Crystal structure and hydrogen-bonding system in cellulose Iβ from synchrotron X-ray and neutron fiber diffraction. J Am Chem Soc 124: 9074–9082. doi:10.1021/ja0257319

Nishiyama Y, Sugiyama J, Chanzy H, Langan P (2003) Crystal structure and hydrogen bonding system in cellulose Iα from synchrotron X-ray and neutron fiber diffraction. J Am Chem Soc 125:14300–14306. doi:10.1021/ja037055w

O'Sullivan A (1997) Cellulose: the structure slowly unravels. Cellulose 4:173–207. doi:10.1023/a:1018431705579

Paavilainen S, Róg T, Vattulainen I (2011) Analysis of twisting of cellulose nanofibrils in atomistic molecular dynamics simulations. J Phys Chem B 115:3747–3755. doi:10.1021/jp111459b

Pan J, Hamad W, Straus SK (2010) Parameters affecting the chiral nematic phase of nanocrystalline cellulose films. Macromolecules 43:3851–3858. doi:10.1021/ma902383k

Parthasarathi R, Bellesia G, Chundawat SPS, Dale BE, Langan P, Gnanakaran S (2011) New insights into hydrogen bonding and stacking interactions in cellulose. J Phys Chem A 115:14191–14202. doi:10.1021/jp203620x

Peralta-Inga Z, Johnson GP, Dowd MK, Rendleman JA, Stevens ED, French AD (2002) The crystal structure of the α-cellobiose 2 NaI 2 H2O complex in the context of related structures and conformational analysis. Carbohydr Res 337(9):851–861. doi:10.1016/S0008-6215(02)00041-1

Perdew JP, Burke K, Ernzerhof M (1996) Generalized gradient approximation made simple. Phys Rev Lett 77:3865–3868. doi:10.1103/PhysRevLett.77.3865

Revol J-F, Godbout L, Gray DG (1998) Solid self-assembled films of cellulose with chiral nematic order and optically variable properties. J Pulp Pap Sci 24:146–149

Řezáč J, Hobza P (2012) Advanced corrections of hydrogen bonding and dispersion for semiempirical quantum mechanical methods. J Chem Theory Comput 8:141–151. doi:10.1021/ct200751e

Scalmani G, Frisch MJ (2010) Continuous surface charge polarizable continuum models of solvation. I. General formalism. J Chem Phys 132:114110. doi:10.1063/1.3359469

Shopsowitz KE, Hao Q, Hamad WY, MacLachlan MJ (2010) Free-standing mesoporous silica films with tunable chiral nematic structures. Nature 468:422–425. doi:10.1038/nature09540

Simon S, Duran M, Dannenberg JJ (1996) How does basis set superposition error change the potential surfaces for hydrogen-bonded dimers? J Chem Phys 105(24):11024–11031. doi:10.1063/1.472902

Stein A (2010) Materials chemistry: thin films with a hidden twist. Nature 468:387–388. doi:10.1038/468387a

Shao Y, Molnar LF, Jung Y, Kussmann J, Ochsenfeld C, Brown ST, Gilbert ATB, Slipchenko LV, Levchenko SV, O'Neill DP, Jr RAD, Lochan RC, Wang T, Beran GJO, Besley NA, Herbert JM, Lin CY, Voorhis TV, Chien SH, Sodt A, Steele RP, Rassolov VA, Maslen PE, Korambath PP, Adamson RD, Austin B, Baker J, Byrd EFC, Dachsel H, Doerksen RJ, Dreuw A, Dunietz BD, Dutoi AD, Furlani TR, Gwaltney SR, Heyden A, Hirata S, Hsu C-P, Kedziora G, Khalliulin RZ, Klunzinger P, Lee AM, Lee MS, Liang W, Lotan I, Nair N, Peters B, Proynov EI, Pieniazek PA, Rhee YM, Ritchie J, Rosta E, Sherrill CD, Simmonett AC, Subotnik JE, III HLW, Zhang W, Bell AT, Chakraborty AK, Chipman DM, Keil FJ, Warshel A, Hehre WJ, III HFS, Kong J, Krylov AI, Gill PMW (2010) Head-Gordon M Spartan '10, Wavefunction, Inc.

Zhao Y, Truhlar DG (2007) The M06 suite of density functionals for main group thermochemistry, thermochemical kinetics, noncovalent interactions, excited states, and transition elements: two new functionals and systematic testing of four M06-class functionals and 12 other function. Theoret Chem Acc 120:215–241. doi:10.1007/s00214-007-0310-x